Synapse

WILEY

SYNAPSE

RESEARCH ARTICLE OPEN ACCESS

Cellular-Resolution and Bulk-Fluorescence Recordings of Calcium Activity Yield Reciprocal Readouts of In Vivo Drug Efficacy

Seongsik Yun | Jones G. Parker

Department of Neuroscience, Northwestern University, Chicago, Illinois, USA

Correspondence: Jones G. Parker (jones.parker@northwestern.edu)

Received: 22 August 2024 | **Revised:** 25 December 2024 | **Accepted:** 3 February 2025

Funding: This study was funded by NIMH K01MH11313201, NINDS R01NS122840, the Whitehall Foundation and National Institutes of Health.

ABSTRACT

Genetically encoded fluorescent sensors of neural activity have become a mainstay of basic neuroscience. However, preclinical drug development has been slower to adopt these tools. Recently, we used miniature microscopes to record Ca^{2+} activity in D1 and D2 dopamine receptor-expressing spiny projection neurons (SPNs) in response to antipsychotic drugs or candidates. Despite the fact that most antipsychotics block D2 receptors, clinical efficacy was associated with the normalization of D1-SPN activity under hyperdopaminergic conditions. In this study, we re-processed these data to approximate a fiber photometry signal and asked whether the conclusions were the same. This re-evaluation is important because fiber photometry has several advantages over cellular-resolution imaging. Consistent with our previous finding that bulk and cellular-resolution imaging report distinct SPN Ca^{2+} dynamics, here the two data types suggested reciprocal effects of drug treatment on D1-SPN and D2-SPN Ca^{2+} activity. While amphetamine treatment increased D1-SPN and decreased D2-SPN Ca^{2+} event rates in cellular-resolution data, it increased the fluorescence of individual neurons but decreased their bulk fluorescence in both cell types. Analyzing detected bulk-fluorescence "events" yielded a closer correlation between the bulk and somatic Ca^{2+} fluorescence. However, it did not fully replicate the results of our previous cellular-resolution recordings following amphetamine or antipsychotic drug treatment. Our results highlight important distinctions between cellular-resolution and bulk measurements of in vivo Ca^{2+} activity. While experimenters using in vivo imaging to understand drug effects on neural activity should heed these distinctions, they should also utilize them to gain a more holistic view of drug action.

1 | Introduction

Recent years have witnessed a rapid expansion in optical tools for monitoring brain function (Patriarchi et al. 2018; Zhang et al. 2023). Today, countless labs routinely deploy user-friendly tools like miniature microscopes and fiber photometry to record neural activity with optical sensors of Ca^{2+} or neurotransmitter release (Cui et al. 2014; Ghosh et al. 2011). This veritable windfall of sensors has empowered scientists to examine fundamental brain processes with unparalleled sensitivity and specificity (Dong et al. 2022).

While the basic research community heartily embraces these optical tools, the drug development community has been slower to adopt in vivo imaging approaches. This is somewhat surprising given the exquisite level of detail offered by these tools, which includes large-scale sampling and high spatial and temporal resolution of specific brain receptor- and cell-subtype dynamics.

Moreover, drug development has long relied on optical readouts for high-throughput screening (Blay et al. 2020). Some of the barriers to implementing in vivo imaging in preclinical drug development include

1) *Technical expertise*: Skillful surgeries and experimental designs are required to obtain quality recordings synchronized to relevant animal behaviors. Expertise in handling, processing, and analyzing large-scale imaging data sets is also necessary to obtain interpretable results.
2) *Financial investment*: The specialized equipment for in vivo imaging is relatively expensive compared to more conventional screening methods like animal behavior. This is particularly true for cellular-resolution approaches like two-photon and miniature microscopy but less applicable to lower resolution ones like fiber photometry. Some of this cost is being offset by open-source solutions, but the price of entry remains a barrier. In the for-profit sector, licensing costs for the genetic tools required to leverage the full capabilities of in vivo imaging are another financial hurdle (transgenic mice, genetically encoded sensors, and other genetic elements).
3) *Timeframe*: In vivo imaging approaches require animals to undergo surgeries (often multiple) with necessary wait times of ≥1 month before experimental testing. These approaches can also require multitransgenic lines with time-consuming breeding schemes (e.g., to image a specific cell type in a specific genetic disease model). Finally, large-scale imaging data sets can take weeks to months to completely process and analyze across subjects, depending on the complexity of the experiment and question.

Combined with the uncertainty of whether in vivo imaging will have greater predictive value than conventional readouts, this (inexhaustive) list of challenges poses a risk to groups considering adopting these tools to understand and advance their drug candidates. However, these challenges are not insurmountable. The number of neuroscientists trained to do in vivo imaging has grown significantly in recent years, and as the field's collective expertise has matured, the timeline to interpretable results has decreased (e.g., reduced surgical failure rates and expedited data processing). Further, more cost-effective approaches like fiber photometry or open-source microscopes have alleviated some of the financial burden (Aharoni et al. 2019; Cui et al. 2014). Fiber photometry also simplifies data processing and analysis, shortening the time it takes to obtain results and cutting down the expertise required to interpret them.

Several groups, including ours, have demonstrated that in vivo imaging can identify unique signatures of therapeutic efficacy (Hirano et al. 2022; Manning et al. 2023; Marshall et al. 2024; Parker et al. 2018). In a recent study, we used miniature microscopes to image cellular-resolution Ca^{2+} activity in response to treatment with antipsychotic drugs and candidates (Yun et al. 2023). We chose to examine antipsychotics because the behavioral phenotypic screens for these drugs have limited predictive value (Spark et al. 2022). Moreover, despite knowing the molecular mechanisms of many different antipsychotic drugs, their circuit-level mechanisms of action are not well understood. Gaining this understanding is important for developing new medicines with the potential to address treatment-resistant psychosis or the intractable negative and cognitive symptoms of schizophrenia (Huhn et al. 2019; Moya et al. 2023).

Our study focused on the striatum, whose principal neurons are spiny projection neurons (SPNs) that express either D1 or D2 dopamine receptors. We know that dopamine is elevated in the dorsal striatum of patients with schizophrenia and that antipsychotic drugs preferentially attenuate D2 receptor signaling (Abi-Dargham et al. 2000; Creese et al. 1996; McCutcheon et al. 2019; Seeman et al. 1976). To study this process, we expressed the genetically encoded Ca^{2+} indicator GCaMP7f in striatal D1-SPNs or D2-SPNs (in separate cohorts of mice) and asked whether antipsychotics preferentially modulate dopamine's effects on D2-SPN activity. Surprisingly, we found that every clinically effective drug we tested normalized dopamine's effects on D1-SPN activity, and the most clinically efficacious drug had no effect on D2-SPN activity at all. Our results have expanded our understanding of antipsychotic drug effects to the level of intact neural circuits (rather than individual receptors). In doing so, the study has established in vivo imaging as a new phenotypic screening tool with the power to bridge molecular and neural circuit-level mechanisms of action.

While our study's proof of concept alleviates some of the uncertainty of investing in these tools for drug development, the experiments were still relatively complex, costly, and time consuming (see points above). Given that in vivo imaging approaches like fiber photometry can circumvent these barriers, here we asked whether re-evaluating the cellular-resolution imaging data from our study in a manner that approximates a fiber photometry signal would yield the same conclusions (Graphical Abstract). This is an important question because we have shown that bulk and cellular-resolution Ca^{2+} imaging in the striatum likely reflect distinct biological processes (Legaria et al. 2022), and observing these processes may provide further insight into the actions of drugs in the brain. Further, because bulk measurements are accessible to more labs, it is important to identify steps that may equate them to our previous analysis of somatic Ca^{2+} activity. In comparing the effects of drug treatment on bulk and somatic D1-SPN and D2-SPN Ca^{2+} activity, we found that the two different analyses yield reciprocal accounts of drug action. We conclude that bulk and cellular-resolution in vivo imaging may be interchangeable in some circumstances, but they provide drastically different representations of pharmacological effects in the brain. We then identified data processing steps to improve the correspondence between the bulk and cellular-resolution imaging data in our study and discussed the advantages of having both data types for discerning the complex effects of systemic pharmacological treatment on neural circuit function.

2 | Methods

All methods and materials except for the bulk-fluorescence signal analysis are identical to our original manuscript (Yun et al. 2023). Here, we briefly summarize those methods and detail any new analysis approaches in the current study.

2.1 | Mice

All mice were housed and handled according to guidelines approved by the Northwestern University Animal Care and Use Committee. We used GENSAT *Drd1a* (FK150) or *Adora2a* (KG139) BAC transgenic Cre-driver mouse lines (www.mmrrc.org), backcrossed to a C57BL/6J background (Jax # 000664). All mice were 12–24 weeks old at the start of experimental testing.

2.2 | Virus Injections

We anesthetized mice with isoflurane (2% in O_2) and stereotaxically injected the virus at a rate of 250 nL·min^{-1} into the DMS using a microsyringe with a 33-gauge beveled tip needle (WPI; Nanofil). After each injection, we left the syringe in place for 5 min, withdrew the syringe 0.1 mm, waited 5 more min, and then slowly withdrew the syringe. We then sutured the scalp, injected analgesic (Buprenorphine SR; 1 mg·kg^{-1}), and allowed the mice to recover for at least 1 week. We injected 500 nL of AAV2/9-Syn-FLEX-GCaMP7f (1.6×10^{12} GC·mL^{-1}; AddGene) at AP: 0.8 mm, ML: 1.5 mm, and DV: −2.7 mm.

2.3 | Implant Surgeries

To prepare mice for Ca^{2+} imaging, we anesthetized virus-injected mice with isoflurane (2% in O_2) and used a 1.4-mm-diameter drill bit to create a craniotomy (AP: 0.8 mm; ML: 1.5 mm) for implanting an optical guide tube. We used a 0.5-mm-diameter drill bit to drill four additional small holes at spatially distributed locations for insertion of four anchoring skull screws (Antrin miniature specialties). We aspirated the cortex down to DV: −2.1 mm from the dura using a 27-gauge, blunt-end needle and implanted the optical guide tube at DV: −2.35 mm from the dura. After placing the guide tube, we applied Metabond (C&B) to the skull and then used dental acrylic (Coltene) to fix the full assembly along with a stainless-steel head-plate (Laser Alliance) for head-fixing mice during attachment and release of the miniature microscope. We injected analgesic (Buprenorphine SR; 1 mg·kg^{-1}) and allowed the mice to recover for 3–4 weeks before mounting the miniature microscope.

2.4 | Miniature Microscope Mounting

We anesthetized mice with ample GCaMP7f expression (2% isoflurane in O_2), placed them into a stereotaxic frame, and glued the GRIN lens in the guide tube with UV light curable epoxy (Loctite 4305). Next, we used the stereotaxic manipulator to lower the miniature microscope with its attached base plate (nVista; Inscopix Inc.) toward the GRIN lens until the fluorescent tissue came into focus. We then created a structure of blue-light curable resin (Flow-It ALC; Pentron) on the dental acrylic skull cap around the base plate, then attached the structure to the miniature microscope base plate using UV curable epoxy. Finally, we coated the epoxy/resin with black nail polish to make it opaque.

2.5 | In Vivo Pharmacology

We administered all drugs via subcutaneous injection (1 mL·kg^{-1} injection volume for SEP-363856 and 10 mL·kg^{-1} injection volume for all other drugs). We administered treatment in blocks consisting of a vehicle, a low dose, and a high dose for Ca^{2+} imaging experiments. All mice received one treatment per day and 1 day off between the different treatment blocks. In the current study, we restricted our analyses to the vehicle and high-dose drug + amphetamine treatment conditions.

We dissolved clozapine (3.2 mg·kg^{-1}) and haloperidol (0.32 mg·kg^{-1}) in 0.3% tartaric acid. We dissolved SCH23390 (0.1 mg·kg^{-1}), SCH39166 (0.32 mg·kg^{-1}), xanomeline (10 mg·kg^{-1}), and D-amphetamine hemisulfate (2.5 mg·kg^{-1}) in saline (0.9% NaCl). We dissolved MP-10 (3.2 mg·kg^{-1}) in 5% 2-hydroxypropyl-β-cyclodextrin in saline, VU0467154 (10 mg·kg^{-1}) in 10% Tween 80, SKF38393 (100 mg·kg^{-1}) in water, and SEP-363856 (10 mg·kg^{-1}) in DMSO. We dissolved olanzapine (3.2 mg·kg^{-1}) in glacial acetic acid and brought it to the desired volume and pH (~6.0) with saline and NaOH. We obtained VU0467154 from the Vanderbilt Center for Neuroscience and Drug Discovery, xanomeline and SEP-363856 from MedChemExpress, and all other drugs/reagents from Sigma.

2.6 | In Vivo Ca^{2+} Imaging

We habituated mice to a circular open-field arena (30.48-cm diameter) for 3 days (1 h per day), during which we also habituated the mice to two subcutaneous injections of saline and one injection of amphetamine (2.5 mg·kg^{-1}). After 20 min of habituation in the open field, we injected mice with vehicle or drug, waited 10 min, and recorded Ca^{2+} activity for 15 min, then injected amphetamine, waited 10 min, and recorded Ca^{2+} activity for 45 min (Figure 3a). We used an illumination power of 50–200 μW at the specimen plane and a 20-Hz image frame-acquisition rate.

2.7 | Behavioral Tracking

We used a TTL-triggered video camera with IC Capture 2.4 software (The Imaging Source) and a varifocal lens (T3Z2910CS; Computar) to record 20-Hz videos of freely moving mouse behavior. We used software written in ImageJ and part of the CIAtah analysis suite (https://bahanonu.github.io/ciatah/) to track each mouse's position in an open-field arena. Using the resulting positional traces, we identified the animal's instantaneous running speed throughout the synchronized recordings of neural activity. We identified the onsets of locomotion as movement bouts that exceeded the movement threshold (0.5 cm·s^{-1}) for a duration of at least 1 s and were preceded by a period of at least 1-s duration below the movement threshold (Figure 2).

2.8 | Ca^{2+} Movie Preprocessing

The "somatic" Ca^{2+} activity processing pipeline and active neuron identification were identical to our previous publication (Yun et al. 2023). For the "bulk" Ca^{2+} activity processing pipeline,

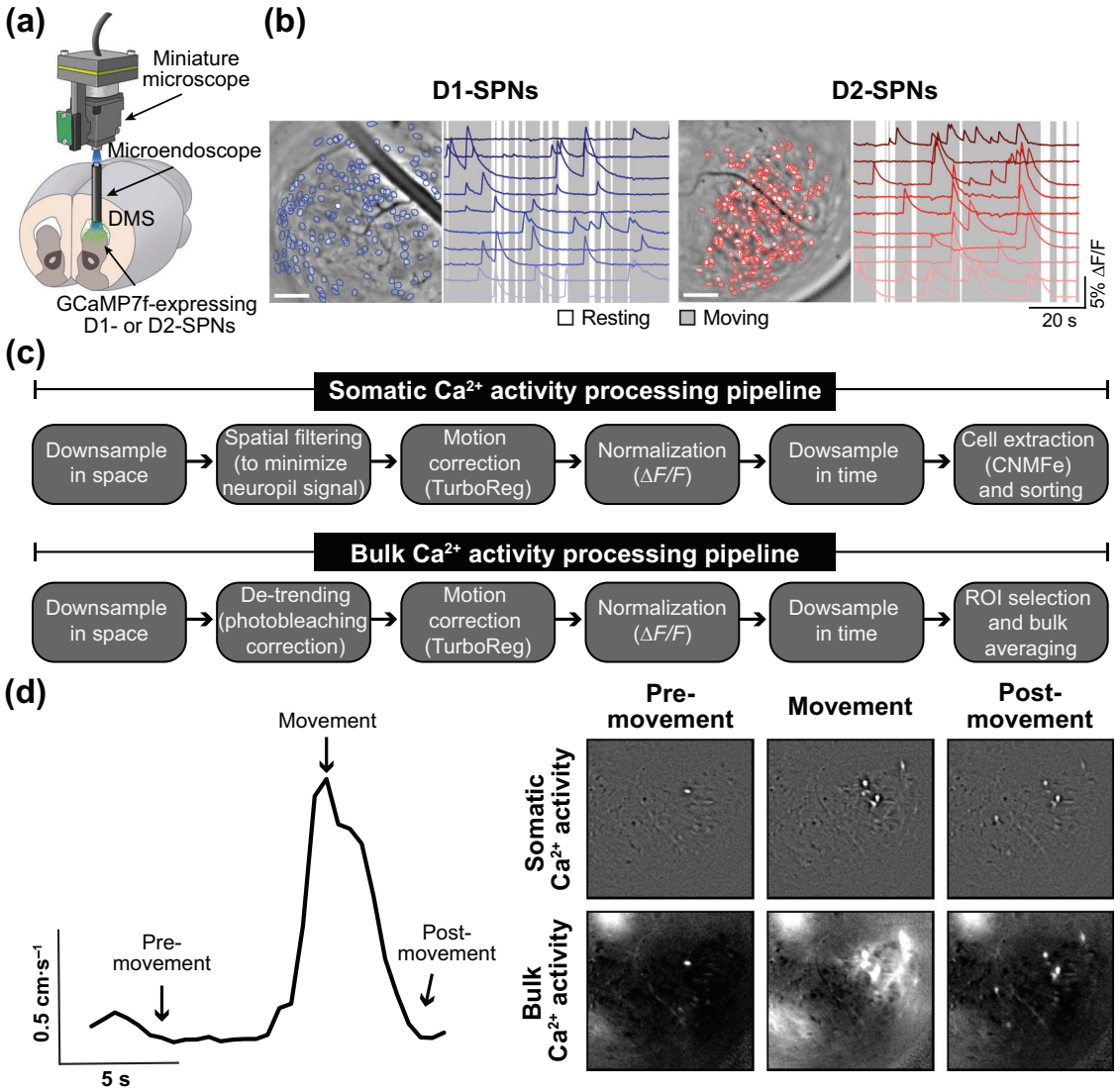

FIGURE 1 | Ca^{2+} imaging in D1-SPNs and D2-SPNs with cellular-resolution and bulk-fluorescence using different data processing pipelines. (a) We used a miniature microscope and microendoscope to image Ca^{2+} activity in D1-SPNs and D2-SPNs by expressing GCaMP7f in the dorsomedial striatum (DMS). (b) Cell centroid locations overlaid on mean fluorescence images of DMS and example Ca^{2+} activity traces from D1-SPNs and D2-SPNs in representative D1-Cre (*left*) and A2A-Cre (*right*) mice. Scale bar: 100 μm. (c) Data processing pipelines for analyzing somatic (*top*) and bulk (*bottom*) Ca^{2+} activity. (d) Example still frames from $\Delta F/F$ movies of Ca^{2+} activity with respect to movement (*left*), processed using the somatic (*top right*) and bulk (*bottom right*) data processing pipelines.

we used the CIAtah analysis suite (Corder et al. 2019) to (1) down-sample the acquired Ca^{2+} movies in space using 2 × 2 bilinear interpolation. We then used a custom Matlab script to (2) correct the movies for any photobleaching by dividing each movie by using exponential fit to the time trace of the average of every pixel in every frame. We used CIAtah to (3) motion correct the movies using the TurboReg algorithm (Thevenaz et al. 1998), (4) compute the $\Delta F/F$ of the movie by subtracting each pixel's average over the entire recording session and dividing by that average in each frame, and (5) temporally down-sample the resulting $\Delta F/F$ movies by a factor of 4 using linear interpolation to a frame rate of 5 Hz. Finally, we used our Matlab script to (6) manually draw a rectangular mask to select the center area of the GRIN lens and exclude areas around the edges of the lens and (7) average all the pixels contained within that mask to calculate the overall mean $\Delta F/F$ trace. The omission of a spatial filtering step was particularly crucial for generating the bulk-fluorescence Ca^{2+} activity traces. For a detailed description of the effects of spatial filtering or its omission on epifluorescence recordings of cellular-resolution Ca^{2+} activity, refer to https://bahanonu.github.io/ciatah/help_spatial_filtering/.

2.9 | Ca^{2+} Event Detection

After processing the movies using the somatic or bulk-fluorescence Ca^{2+} activity pipelines, we identified the individual "events" in each individual cell's CNMFe trace or the bulk-fluorescence trace using a threshold-crossing algorithm (Corder et al. 2019). We removed noise and reduced fluctuations in baseline fluorescence by averaging over a 600-ms (three frames) sliding window, then subtracting a median-filtered version (40-s

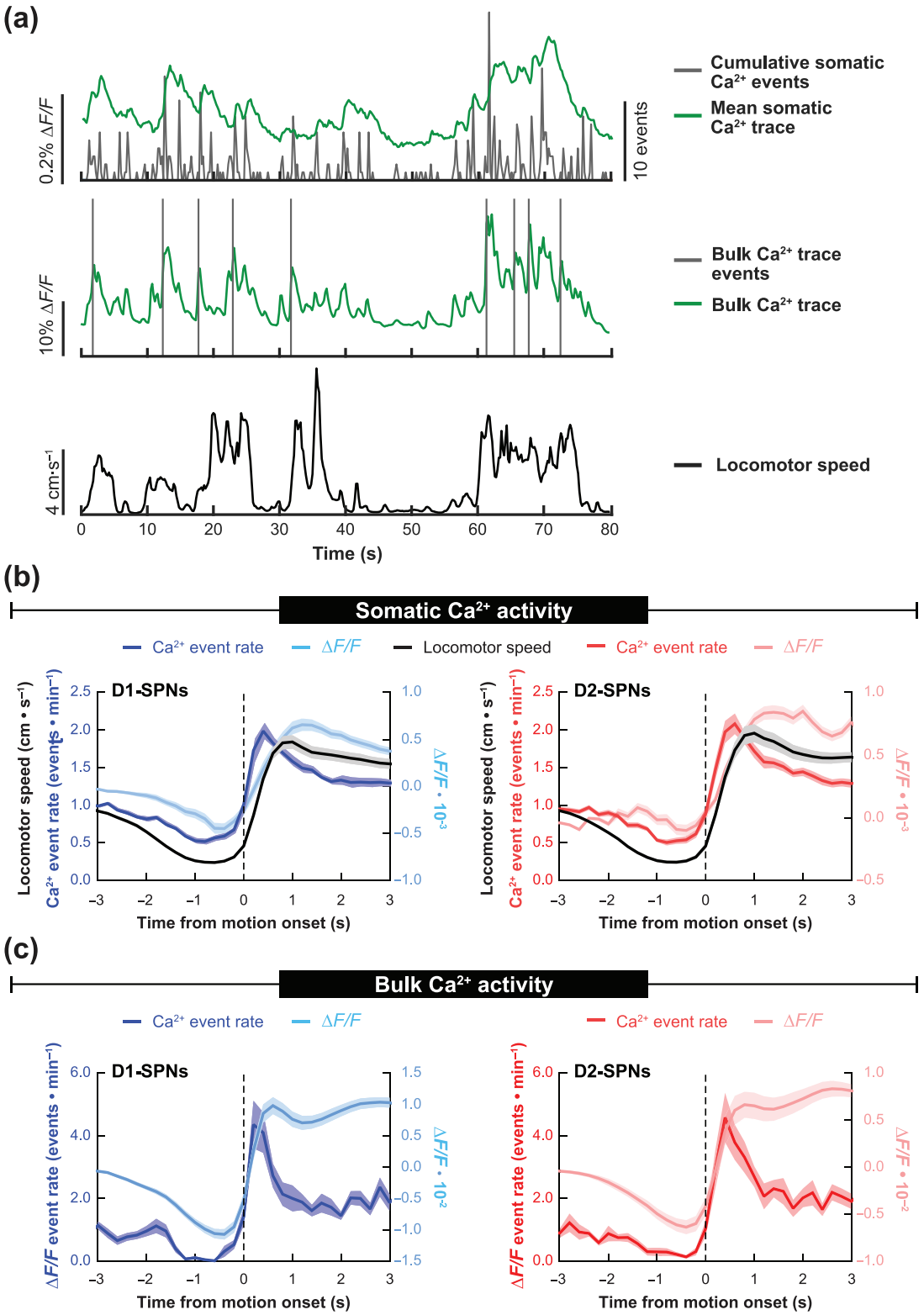

FIGURE 2 | Example somatic and bulk-fluorescence traces and their detected events in relation to movement. (a) Example somatic fluorescence and event traces of somatic (*top*) and bulk (*middle*) Ca^{2+} activity, along with the corresponding locomotor speed trace from a single mouse (*bottom*). (b) Locomotor speed, Ca^{2+} event rates, and Ca^{2+} activity trace ($\Delta F/F$) of individual D1-SPNs and D2-SPNs relative to motion onset processed using the somatic Ca^{2+} activity processing pipeline. (c) Bulk-fluorescence Ca^{2+} activity trace ($\Delta F/F$) and bulk-fluorescence Ca^{2+} event rates of D1-SPNs and D2-SPNs relative to motion onset processed using the bulk Ca^{2+} activity processing pipeline. Data in panels (b) and (c) are expressed as mean ± SEM from $N = 18$ D1-Cre and $N = 17$ A2A-Cre mice.

sliding window) of the trace from the smoothed version. We calculated the standard deviation (SD) of the resulting trace and identified any peaks that were ≥2.5 SD above baseline noise for somatic and ≥1.5 SD for the bulk-fluorescence traces of Ca^{2+} activity while enforcing a minimum interevent time of >1.6 s. We determined the initiation time of each Ca^{2+} event as the temporal midpoint between the time of each event's fluorescence peak and the most recent preceding trough in fluorescence. All analyses of somatic Ca^{2+} activity used either the resulting 5-Hz binarized event trace or the input somatic $\Delta F/F$ traces, and analysis of bulk-fluorescence used either the 5-Hz $\Delta F/F$ or the binarized bulk-fluorescence event trace. To generate the illustrative somatic Ca^{2+} activity traces in Figures 1b and 2a (*top*), for each example cell, we set to zero all pixels of the cell's spatial filter with weights <50% of the maximum value in the filter and then applied the truncated filter to the $\Delta F/F$ movie to generate a Ca^{2+} activity trace.

2.10 | Analysis of Ca^{2+} Imaging Data at Motion Onset

For the analysis of somatic Ca^{2+} activity, we first averaged a 10-s window of each neuron's event or $\Delta F/F$ trace across all instances of motion onset. We then calculated each neuron's baseline activity as the mean event rate or $\Delta F/F$ during the interval from −5 to −2 s before motion onset (across all motion onsets) and averaged baseline activity across all neurons. We then divided each cell's mean event trace (across all motion onsets) by the average baseline event rate of all cells or subtracted from each cell's mean $\Delta F/F$ trace (across all motion onsets) the mean baseline $\Delta F/F$ of all cells (Figure 2b). We performed the same analyses for the bulk-fluorescence Ca^{2+} event and $\Delta F/F$ traces as single trace data, averaging each across all instances of motion onset and normalizing to baseline event rate or $\Delta F/F$ by division or subtraction, respectively (Figure 2c).

2.11 | Analysis of Ca^{2+} Activity as a Function of Locomotor Speed

For the analysis of somatic Ca^{2+} activity, we used the binarized event or the $\Delta F/F$ traces of each cell and averaged these values across all cells in each mouse as a function of their locomotor speed using increasing speed bin sizes following vehicle and amphetamine treatment, as shown in Figure 4a,b (*left*). We normalized the values in each speed bin to the corresponding values following vehicle treatment by division (event data) or subtraction ($\Delta F/F$ data), then averaged the speed bins during periods of rest and movement to generate the bar plots in Figure 4a,b (*right*). We performed the same analyses for the bulk-fluorescence Ca^{2+} $\Delta F/F$ and event traces but did not average across cells as they were singular traces (Figure 4c,d).

To compute the correlations between the different data analysis types, we first normalized the different data in Figure 4, computed as a function of locomotor speed. For the event trace analysis data, we divided the values following amphetamine treatment by their corresponding speed-bin value following vehicle treatment (Figure 5a). For the bulk analysis data, we first added the minimum value in each mouse's vehicle or amphetamine cellular or bulk $\Delta F/F$ versus speed trace to all values in that mouse's cellular or bulk $\Delta F/F$ versus speed trace to eliminate negative values before normalization. After shifting the traces such that none of their values were <0, we divided the values following amphetamine treatment by their corresponding speed-bin value following vehicle treatment (Figure 5a). Finally, we computed the Pearson correlation coefficient between the different, normalized calculations of Ca^{2+} activity versus speed using the Matlab "corr" function (Figure 5b).

2.12 | Data Analysis and Statistical Tests

We performed data analysis using MATLAB (2019b) and ImageJ (1.53k). We used Prism 9 (GraphPad) to perform statistical tests. For paired tests, we used Wilcoxon signed-rank tests or one-way repeated measures ANOVA. For post hoc tests, we used a Holm–Sidak correction for multiple comparisons.

2.13 | Data Availability

Most of the source data for this manuscript are provided in the previous publication (Yun et al. 2023). Any source data generated through the re-analyses presented here are available from the corresponding author upon request.

3 | Results

3.1 | Data Processing Pipelines for Generating "Somatic" and "Bulk-Fluorescence" SPN Ca^{2+} Activity Traces

As previously reported, we virally expressed the fluorescent Ca^{2+} indicator GCaMP7f in the DMS of *Drd1a*^{Cre} (D1-Cre) or *Adora2a*^{Cre} (A2A-Cre) mice (Yun et al. 2023). We then implanted an optical guide tube and microendoscope into the DMS and mounted the mice with a miniature fluorescence microscope to record D1-SPN or D2-SPN activity (Figure 1a). This approach allowed us to monitor Ca^{2+} activity in hundreds of individual D1-SPNs and D2-SPNs in freely behaving mice (Figure 1b). In our previous study, we used a data processing pipeline that included dividing each Ca^{2+} imaging movie frame by its low-pass-filtered version to minimize contamination from GCaMP7f activity in neuropil or out-of-focus cells (Figure 1c; *top*). In the current study, to approximate a bulk-fluorescence, fiber photometry signal in these cellular resolution recordings, we used a movie processing pipeline in which we omitted this spatial filtering step (Figure 1c; *bottom*). This resulted in cellular-resolution Ca^{2+} imaging movies that retained their apparent, large-field fluctuations in fluorescence intensity (Movie S1). We also included a photobleaching correction step to correct for any slow decay in full-field fluorescence. After these processing steps, we manually chose a single region of interest (ROI) that incorporated as much of the field of view as possible while avoiding the edges of the microendoscope to compute a bulk-fluorescence trace. Figure 1d shows example single-frame images from the same movie from an individual mouse processed using

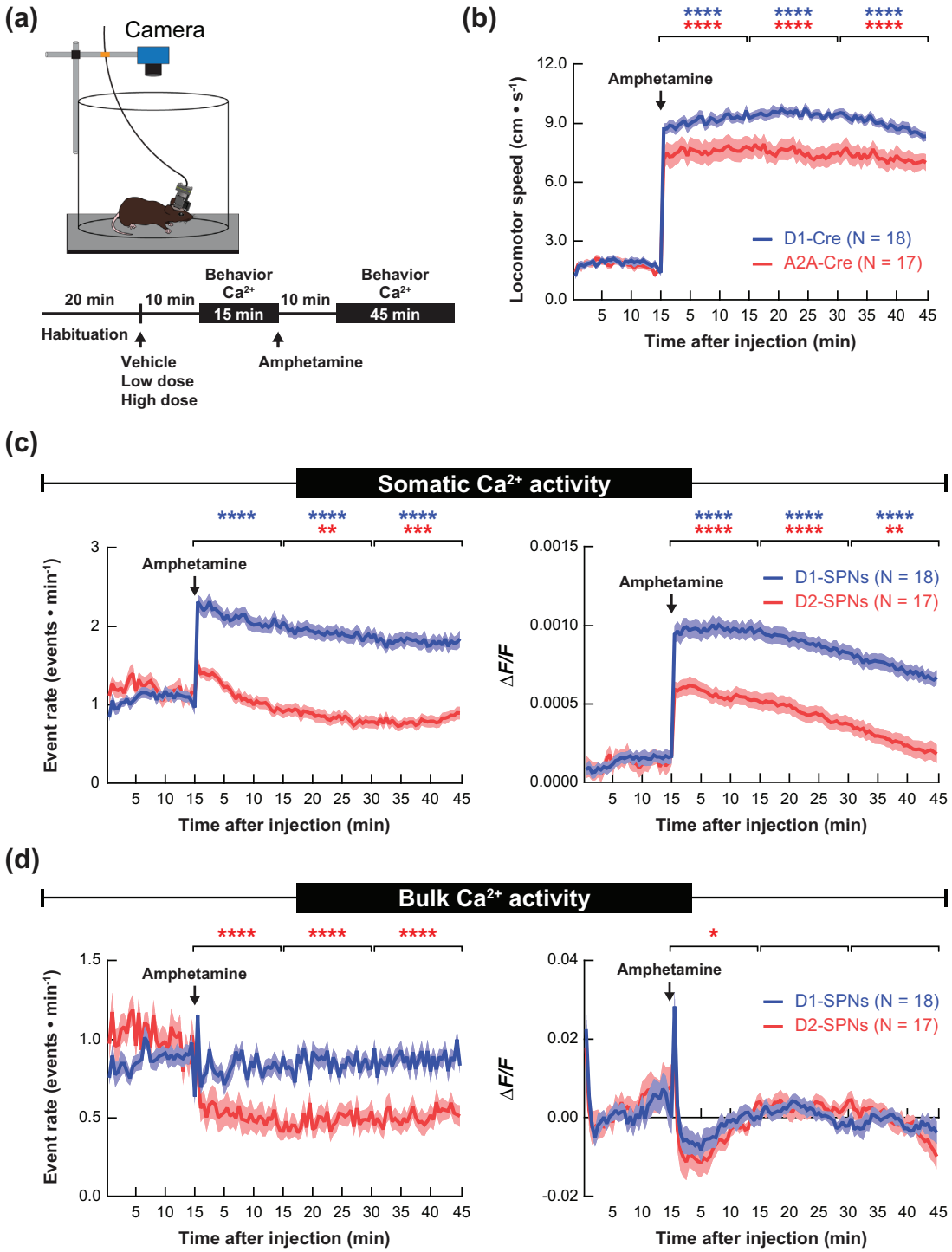

FIGURE 3 | Different analyses of D1-SPN and D2-SPN Ca^{2+} activity yield reciprocal accounts of amphetamine treatment effects. (a) Schematic of drug treatment schedule and behavior and neural recording schedule in the open-field arena. (b) Locomotor speed during the 15-min recording period following vehicle treatment and the 45-min recording period after amphetamine treatment. (c) Somatic Ca^{2+} event rates (*left*) and fluorescence ($\Delta F/F$) (*right*) of D1-SPN and D2-SPN activity, averaged across all neurons in each mouse, following vehicle or amphetamine treatment. (d) Bulk-fluorescence Ca^{2+} event rates (*left*) and Ca^{2+} activity bulk-fluorescence ($\Delta F/F$) (*right*) of D1-SPN and D2-SPN activity following vehicle or amphetamine treatment. Data are expressed as mean ± SEM from $N = 18$ D1-Cre and $N = 17$ A2A-Cre mice. ****$p < 10^{-4}$, ***$p < 10^{-3}$, **$p < 10^{-2}$, and *$p < 0.05$; two-way ANOVA with Holm–Sidak's multiple comparison test compared to the 15-min vehicle treatment period.

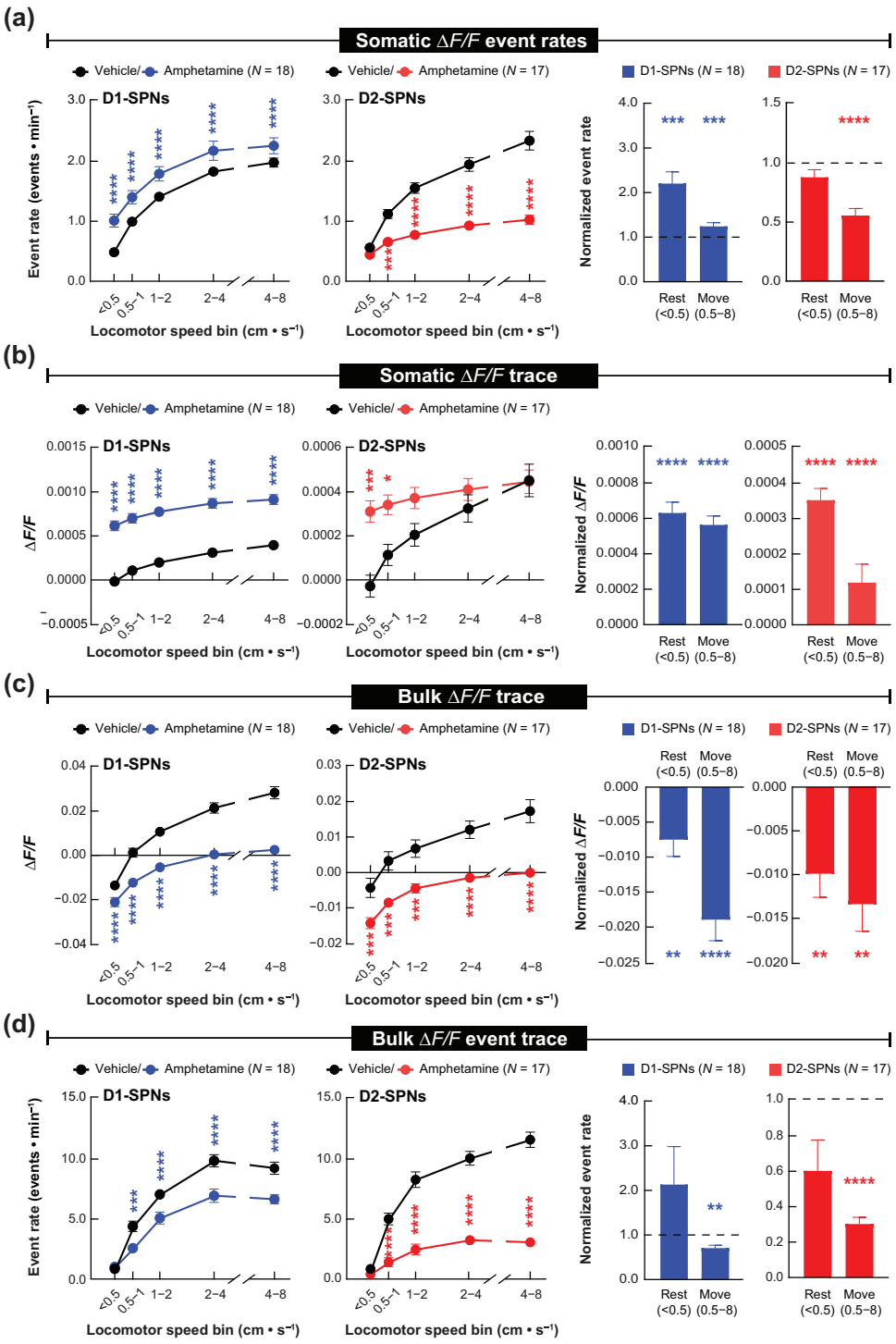

FIGURE 4 | Effects of amphetamine treatment on D1-SPN and D2-SPN Ca^{2+} activity analyzed in four different ways as a function of locomotor speed. (a, b) Effects of vehicle or amphetamine treatment on somatic D1-SPN and D2-SPN Ca^{2+} event rates (a) and fluorescence ($\Delta F/F$) (b) across increasing locomotor speed bins (*left*) or averaged across resting (<0.5 cm·s^{-1}) and moving (0.5–8 cm·s^{-1}) speed bins and normalized to mean values following vehicle treatment (*right*). (c, d) The same analyses of Ca^{2+} activity with respect to spontaneous movement in panels (a) and (b), but for bulk-fluorescence ($\Delta F/F$) (c) and bulk-fluorescence events (d). Data are expressed as mean ± SEM ($N = 18$ D1-Cre and $N = 17$ A2A-Cre mice; ****$p < 10^{-4}$, ***$p < 10^{-3}$, and **$p < 0.01$ for comparison to vehicle treatment; two-way ANOVA with Holm–Sidak's multiple comparison test for b–d line plots; Wilcoxon, two-tailed signed-rank test for the bar plots.

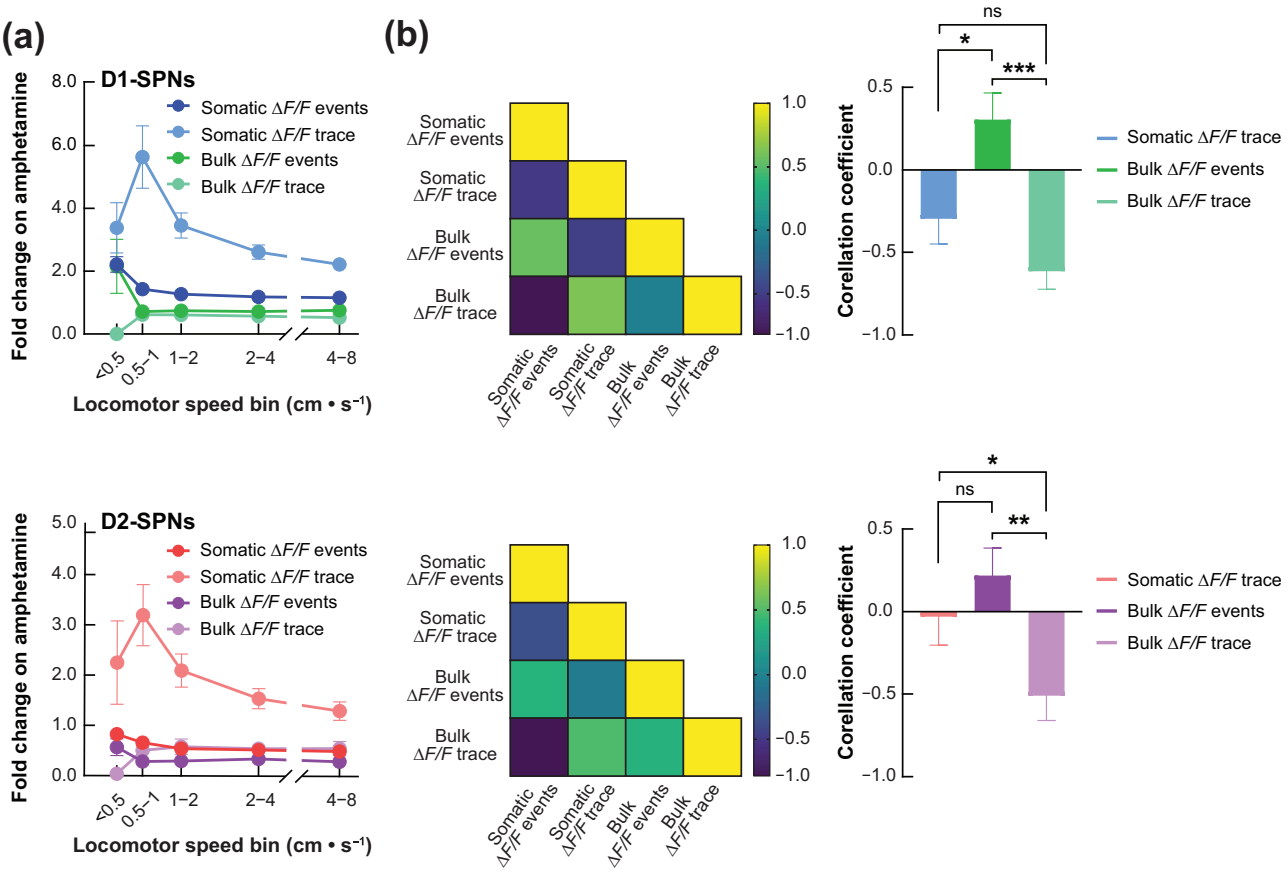

FIGURE 5 | Correlations between somatic and bulk analyses of amphetamine treatment effects on SPN Ca^{2+} activity versus locomotor speed. (a) Fold change in amphetamine treatment-induced D1-SPN (*top*) and D2-SPN (*bottom*) Ca^{2+} activity, calculated as amphetamine/vehicle in each speed bin (see Section 2). (b) Pearson correlation coefficients between the four different analyses of Ca^{2+} activity versus speed (*left*) and statistical comparisons of the correlation coefficients to the analysis of somatic Ca^{2+} event data (*right*). Data are mean ± SEM from $N = 18$ D1-Cre and $N = 17$ A2A-Cre mice (***$p < 10^{-3}$, **$p < 0.01$, and *$p < 0.05$; one-way ANOVA with Holm–Sidak's multiple comparison test).

the somatic and bulk data processing pipelines with respect to an instance of motion onset. Note the more pronounced background fluorescence in the bulk compared to the somatic frames, which underwent spatial filtering to minimize nonsomatic fluorescence.

3.2 | Somatic Versus Bulk-Fluorescence SPN Ca^{2+} Responses in Relation to Spontaneous Movement

First, we analyzed the dynamics of somatic and bulk Ca^{2+} activity with respect to spontaneous movement in the open field during periods of saline treatment. Both the somatic and bulk-fluorescence $\Delta F/F$ traces of Ca^{2+} activity exhibited correlations with movement (Figure 2a). To further examine this relationship, we computed the average somatic and bulk Ca^{2+} activity at the time of motion onsets. On average, somatic Ca^{2+} traces ($\Delta F/F$) and events increased with locomotor speed during motion onset in both D1-SPNs and D2-SPNs (Figure 2b). Likewise, both bulk-fluorescence Ca^{2+} traces ($\Delta F/F$) and events were correlated to speed during motion onset (Figure 2c). These data are consistent with earlier studies examining somatic and bulk SPN Ca^{2+} dynamics with respect to movement initiation (Cui et al. 2013; Parker et al. 2018).

3.3 | Somatic Versus Bulk Ca^{2+} Activity Readouts of Normal and Hyperdopaminergic SPN Dynamics

We recorded behavior and D1-SPN or D2-SPN Ca^{2+} activity following treatment with either vehicle or drug followed by treatment with the dopamine-releasing drug amphetamine (Figure 3a). Amphetamine treatment increased locomotor activity in both D1-Cre and A2A-Cre mice (Figure 3b). The rate of somatic Ca^{2+} events (averaged across all neurons in each mouse) increased in D1-SPNs and decreased in D2-SPNs after amphetamine treatment, consistent with our previous report (Yun et al. 2023) (Figure 3c; *left*). By contrast, in both D1-SPNs and D2-SPNs, amphetamine treatment increased the average somatic $\Delta F/F$, though the increase was less pronounced in D2-SPNs (Figure 3c; *right*). In the bulk Ca^{2+} activity data, amphetamine treatment transiently decreased the $\Delta F/F$ traces of both D1-SPNs and D2-SPNs (Figure 3d; *right*) while decreasing the rate of bulk events in D2-SPNs with negligible effects on the bulk event rate of D1-SPNs (Figure 3d; *left*). Altogether, the same data, when analyzed in four different ways, yielded four completely different depictions of amphetamine treatment's effects on D1-SPN and D2-SPN Ca^{2+} activity.

We know that accounting for locomotor state is crucial when adjudicating the effects of drugs that alter locomotion on D1-

SPN and D2-SPN Ca^{2+} activity because activity in both cell types scales with running speed (Parker et al. 2018; Yun et al. 2023). We previously showed that amphetamine treatment increases somatic Ca^{2+} activity in D1-SPNs and decreases it in D2-SPNs, effects that are most pronounced during periods of rest and movement, respectively (Figure 4a). In contrast to these event rate data, amphetamine treatment uniformly increased somatic but decreased bulk $\Delta F/F$ in both D1-SPNs and D2-SPNs (Figure 4b,c). Analyzing the rate of bulk $\Delta F/F$ events as a function of locomotor speed replicated our original finding that amphetamine suppresses D2-SPN activity (Figure 4a,d). Although the effects of amphetamine treatment on bulk $\Delta F/F$ events in D1-SPNs were more similar to our analysis of somatic Ca^{2+} events, neither of the bulk analyses replicated the increase in D1-SPN activity seen in either of the somatic analyses (Figure 4a–d). In summary, while every analysis type demonstrated a scaling of D1-SPN and D2-SPN Ca^{2+} activity with locomotor speed, each offered a different account of amphetamine treatment's effects on their activity.

To determine how these amphetamine-driven changes in Ca^{2+} activity as a function of running speed relate to our previous analysis of somatic Ca^{2+} events, we normalized the amphetamine to vehicle treatment conditions (by division) in the data plotted in Figure 4. To eliminate negative values in the somatic and bulk $\Delta F/F$ data, we first added the absolute value of the minimum data point (in either the vehicle or amphetamine treatment trace) to every other point in the two traces, such that the minimum value became zero for the pair of treatment condition traces for each mouse. These normalized comparisons yielded a fold change in the effects of amphetamine treatment on Ca^{2+} activity as a function of locomotor speed to the four data types (Figure 5a). Next, we computed the Pearson correlation coefficient between each data analysis type (somatic events, somatic $\Delta F/F$, bulk $\Delta F/F$, and bulk events; Figure 5b). For both D1-SPNs and D2-SPNs, amphetamine's effects on the rate of bulk events best correlated to its effects on the rate of somatic events—even more so than the somatic $\Delta F/F$ (Figure 5b). Therefore, in subsequent analyses, we compared drug effects on somatic and bulk event rates to assess their equivalency for these drug screening experiments.

3.4 | Somatic and Bulk SPN Ca^{2+} Dynamics Differ in Response to Drug Treatment

Dopamine release is increased in the dorsal striatum of patients with schizophrenia (Abi-Dargham et al. 2000; McCutcheon et al. 2019). Previously, we found that clinically effective antipsychotic drugs suppress D1-SPN hyperactivity in the dorsal striatum, specifically under hyperdopaminergic conditions (Yun et al. 2023). Here, we sought to determine whether analyzing bulk-fluorescence data recapitulates this conclusion. Specifically, we focused on the effects of drug treatment on the rates of somatic and bulk-fluorescence Ca^{2+} events—since the latter best correlated with the former, our original metric of drug efficacy (Figure 5b) (Yun et al. 2023). In our somatic, event rate analysis, effective antipsychotic drugs suppressed amphetamine-induced D1-SPN hyperactivity and increased or had no effect on D1-SPN activity levels in the absence of amphetamine treatment (Yun et al. 2023) (Figures 6 and 7; *left*). However, analysis of the rate of bulk-fluorescence events did not fully reproduce this result. Specifically, the bulk event data failed to replicate any of the effects of drug treatment on amphetamine-driven somatic D1-SPN hyperactivity (Figure 6; *right*). For example, while D1R partial agonist (SKF38393) treatment increased somatic D1-SPN activity, it decreased the rate of bulk-fluorescence Ca^{2+} events in D1-SPNs (Figure 7; *right*). Similarly, although the effects of drug treatment on D2-SPN activity were largely consistent between the bulk and somatic analyses during amphetamine treatment (Figure 6), the effects of drug treatment alone on somatic D2-SPN activity were absent in the bulk analysis (Figure 7; *right*). In summary, the analysis of bulk Ca^{2+} activity failed to fully replicate the cellular-resolution analysis, even when focusing on the rate of bulk events. This discrepancy was particularly notable for the D1-SPN data during amphetamine treatment and the D2-SPN data during drug-only treatment.

One metric in our previous study that accurately reflected clinical antipsychotic efficacy was the ratio of drug effects on the rate of somatic D1-SPN Ca^{2+} events activity under hyperdopaminergic versus normal conditions. For example, haloperidol, olanzapine, and clozapine all decreased somatic D1-SPN hyperactivity during amphetamine treatment but increased somatic D1-SPN activity following treatment with each drug alone (Figures 6 and 7; *left*). Likewise, ineffective drugs either exacerbated D1-SPN hyperactivity during amphetamine treatment (MP-10) or dramatically suppressed D1-SPN activity during drug-only treatment (D1 antagonists). Here, to capture these state-dependent effects, we computed an index of neuromodulation by dividing each drug's effects on D1-SPN or D2-SPN activity following amphetamine treatment by its effects following drug-only treatment (Figure 8a). In the most conventional interpretation, drugs with lower values in this state-dependence index of D1-SPN modulation and higher values for D2-SPN modulation are more state-dependent countermodulators of excess dopamine.

Computing this metric on the somatic Ca^{2+} event data resulted in a clear segregation between clinically effective and ineffective antipsychotics, based on their state-dependent effects on D1-SPN activity (Figure 8a). In this analysis, clozapine, the most clinically effective drug we tested, had the lowest ratio of the clinically used drugs. Interestingly, the D1R partial agonist we tested had a similar state-dependent modulation index to clozapine. Although not every drug was significantly different from vehicle, the trend was that effective antipsychotics had lower and ineffective drugs had higher state-dependent indices of D1-SPN modulation (Figure 8a*; left*). By contrast, the state-dependence index of drug effects on somatic D2-SPN activity did not reliably segregate the clinically effective and ineffective drugs (Figure 8a*; right*).

When we performed the same analysis using the rates of bulk Ca^{2+} events, we saw a similar segregation between the clinically effective and ineffective drugs in terms of their effects on bulk activity in D1-SPNs (Figure 8b; *left*). However, these effects did not reach significance, and the metric failed to group the novel antipsychotic xanomeline with the other clinically effective drugs. Like the metric computed on somatic Ca^{2+} activity, the state-dependent indices of drug effects on bulk D2-SPN events also did not separate the effective from the ineffective drugs. Taken together, these results highlight the differences between using cellular-resolution Ca^{2+} activity and using bulk-fluorescence Ca^{2+} activity to discern drug effects on neural

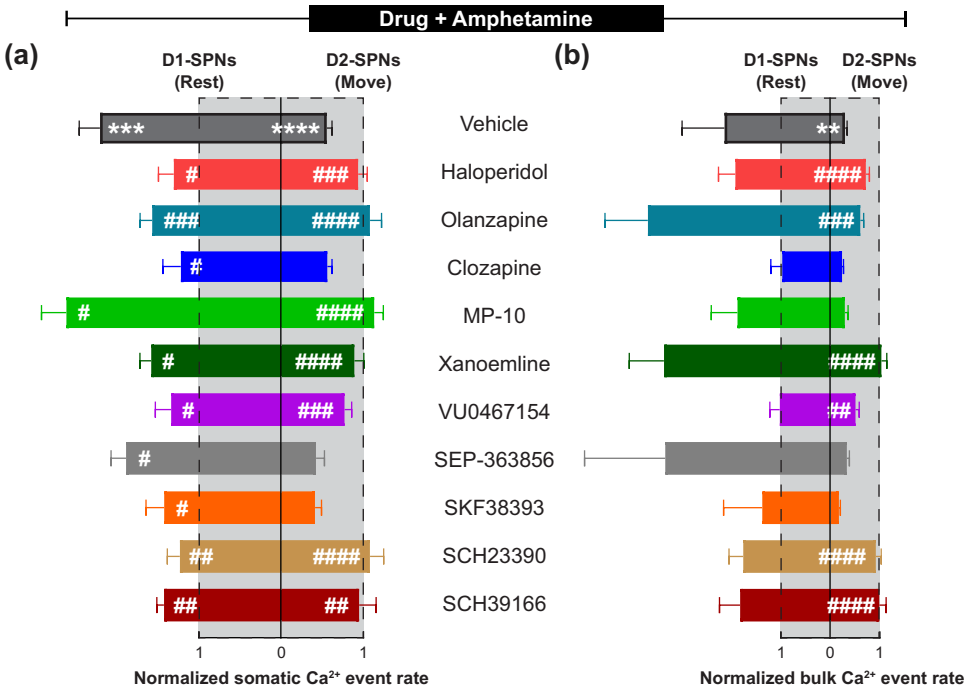

FIGURE 6 | Drug effects on somatic and bulk D1-SPN and D2-SPN Ca^{2+} events under hyperdopaminergic conditions. (a, b) Somatic (a) and bulk-fluorescence (b) Ca^{2+} event rates for D1-SPNs and D2-SPNs following vehicle or high dose of drug + amphetamine treatment, normalized to values following vehicle-only treatment during periods of rest for D1-SPNs and movement for D2-SPNs. Data are mean ± SEM from $N = 7$–11 D1-Cre and $N = 7$–10 A2A-Cre mice (***$p < 10^{-3}$ and **$P < 0.01$ for comparison to vehicle treatment; $^{\#\#\#\#}P < 10^{-4}$, $^{\#\#\#}P < 10^{-3}$, $^{\#\#}P < 10^{-2}$, and $^{\#}P < 0.05$ compared to vehicle + amphetamine treatment; one-way ANOVA with Holm–Sidak's multiple comparison test).

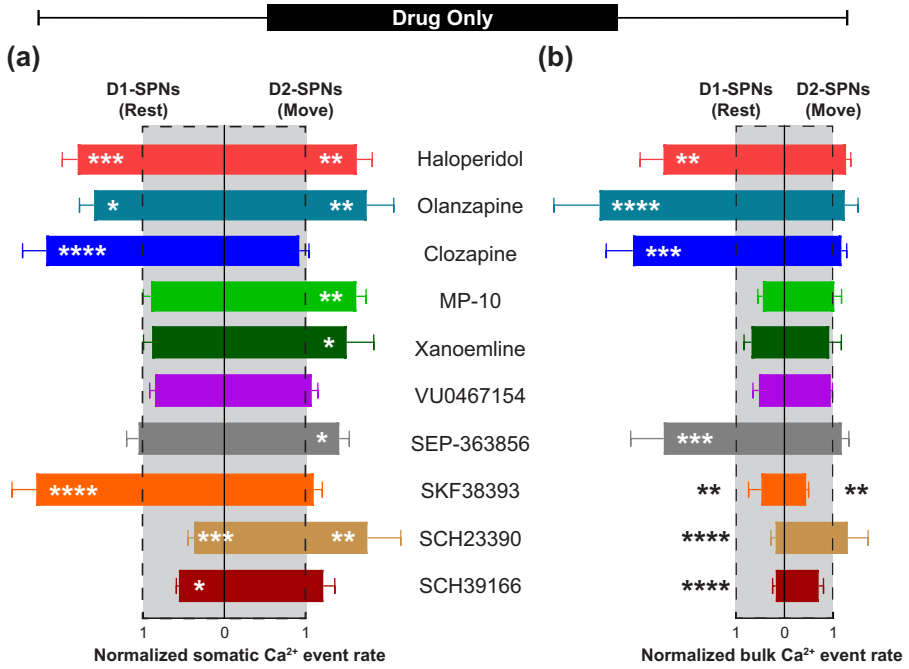

FIGURE 7 | Drug effects on somatic and bulk D1-SPN and D2-SPN Ca^{2+} events under normal conditions. (a, b) Somatic (a) and bulk-fluorescence (b) Ca^{2+} event rates for D1-SPNs and D2-SPNs following vehicle or high dose of drug treatment, normalized to values following vehicle-only treatment during periods of rest for D1-SPNs and movement for D2-SPNs. Data are mean ± SEM from $N = 7$–11 D1-Cre and $N = 7$–10 A2A-Cre mice (****$p < 10^{-4}$, ***$p < 10^{-3}$, **$p < 0.01$, and *$p < 0.05$ for comparison to vehicle treatment; one-way ANOVA with Holm–Sidak's multiple comparison test).

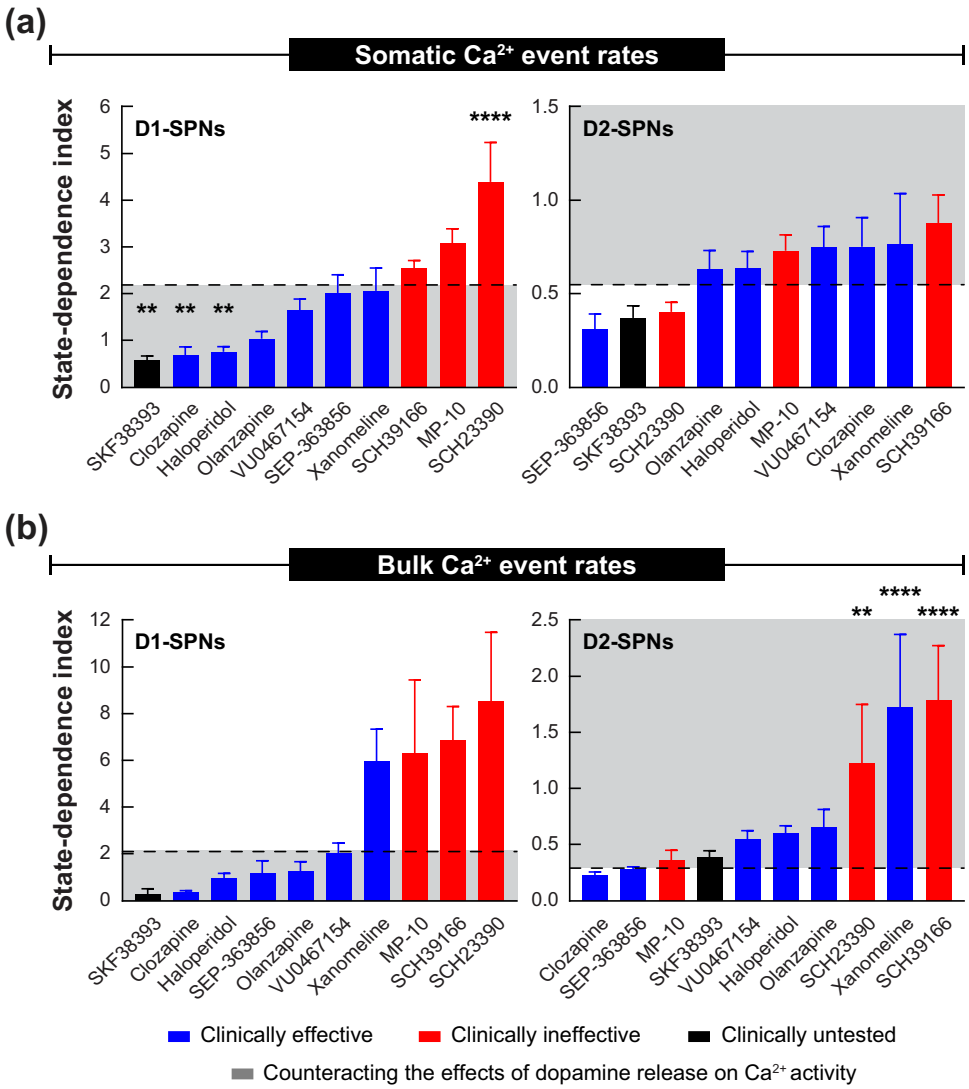

FIGURE 8 | Dopaminergic state-dependent effects of drug treatment on somatic and bulk D1-SPN and D2-SPN Ca^{2+} activity. (a, b) We computed the mean population somatic (a) or bulk-fluorescence (b) event rates during periods of rest for D1-SPNs and movement for D2-SPNs following treatment with vehicle, drug alone, vehicle + amphetamine, or drug + amphetamine. We normalized the values under the latter three treatment conditions to the value following vehicle-only treatment for each mouse. We then took the ratio of these normalized values during amphetamine treatment to the normalized values during drug-alone treatment to obtain a dopaminergic state-dependent index of neuromodulation (high/normal dopamine) for each drug as represented in the two data types [(event rates during vehicle/drug + amphetamine treatment, normalized to vehicle treatment alone levels) / (event rates during drug alone treatment, normalized to vehicle treatment alone levels)]. Data are mean ± SEM from $N = 7$–11 D1-Cre and $N = 7$–10 A2A-Cre mice (****$p < 10^{-4}$ and **$p < 0.01$ for comparison to vehicle treatment; one-way ANOVA with Holm–Sidak's multiple comparison test).

activity. In exploring these different data formats in the context of our earlier study (Yun et al. 2023), we identified steps that better align the two modalities, such as analyses of event detection and state-dependent modulation. This exploration underscores the different information provided by cellular-resolution and bulk-florescence measurements of drug effects on Ca^{2+} activity that, when analyzed together, provide a more holistic readout of drug actions in the brain.

3.5 | Discussion

We have a wealth of information about the in vitro brain receptor-binding profiles of different antipsychotic drugs, but receptor-binding profiles, alone, are insufficient for inferring clinical efficacy (Huhn et al. 2019; Lange et al. 2007; Olten and Bloch 2018). This shortcoming highlights the complex interactions between systemically administered, polypharmacological drugs and the brain. For instance, antipsychotic drugs are thought to attenuate D2R signaling in the dorsal striatum, a brain area where dopamine levels are increased in patients with schizophrenia (Abi-Dargham et al. 2000; Creese et al. 1996; McCutcheon et al. 2019; Seeman et al. 1976). However, in the dorsal striatum alone, D2Rs are expressed in D2-SPNs, in cholinergic interneurons, and on the axon terminals of dopamine neurons that innervate the structure. Further, each of these neurons is reciprocally connected and expresses many other receptors also bound by antipsychotic drugs. Therefore, other than the basic understanding that they attenuate D2R signaling, the mechanism(s) by

which antipsychotic drugs influence brain function to exert their therapeutic effects remains opaque.

Given that antipsychotics are ineffective for ~30% of patients, have adverse side effects, and fail to fully address the cognitive and negative symptoms of schizophrenia, it is imperative to gain a more holistic understanding of how they act on the brain. With its many advantages, in vivo imaging is well-suited to uncovering these details. In particular, the ability to record activity in genetically defined neuronal populations or combine neuromodulator sensors with Ca^{2+} imaging offers a rich perspective of drug actions in the brain. To this end, we asked how 10 different drugs or drug candidates modulate D1-SPNs and D2-SPNs under normal and hyperdopaminergic conditions. Underscoring the informative power of in vivo Ca^{2+} imaging, our cellular-resolution recordings of D1-SPN and D2-SPN activity revealed a previously unappreciated role for the modulation of D1-SPNs by antipsychotic drugs, even though the neurons do not express the receptors principally targeted by those drugs (D2Rs).

As enlightening as these experiments were, they were also time-consuming, laborious, and expensive. Therefore, we sought to determine whether a more straightforward but lower resolution imaging approach might substitute for cellular-resolution imaging in our study. Using similar analytical approaches, we previously showed that fiber photometry in the striatum does not reliably reflect somatic activity as measured by simultaneous electrophysiology and bulk Ca^{2+} imaging in the striatum (Legaria et al. 2022). In the same study, we also compared the relationship between bulk and cellular Ca^{2+} activity using miniature microscope data and concluded that bulk-fluorescence recordings in the striatum better reflect Ca^{2+} activity in neuropil than cell somas in the striatum. The ability to simultaneously measure these two biological processes—Ca^{2+} activity in cell somas and processes—in cellular-resolution recordings offers additional insights into drug action that would not be possible when analyzing either measure alone. At the same time, it suggests that bulk Ca^{2+} recordings may not recapitulate the conclusions of our previous study, which focused on drug effects on somatic D1-SPN and D2-SPN Ca^{2+} event rates.

In terms of spontaneous movement in the open-field arena, both somatic and bulk measures of Ca^{2+} activity increased at motion onset and scaled with locomotor speed, regardless of whether analyzing events or $\Delta F/F$ (Figure 2 and vehicle treatment data in Figure 4). These data are consistent with our previous cellular-resolution recordings and the bulk recordings of D1-SPN and D2-SPN Ca^{2+} activity by others (Cui et al. 2013; Parker et al. 2018). By contrast, we observed stark differences in how amphetamine altered D1-SPN and D2-SPN activity between the different Ca^{2+} imaging analysis formats (Figures 3 and 4). Surprisingly, none of the analysis formats (somatic $\Delta F/F$, bulk $\Delta F/F$, or bulk events) replicated amphetamine's effects on somatic D1-SPN and D2-SPN Ca^{2+} events in our previous study (an increase in D1-SPN and decrease in D2-SPN Ca^{2+} event rates). Even the analysis of somatic $\Delta F/F$ was strikingly different from our previous analysis, even though both analyzed somatic Ca^{2+} activity. Specifically, amphetamine treatment increased the levels of somatic fluorescence in both D1-SPNs and D2-SPNs, even after controlling for changes in locomotor speed (Figure 4a,b). Although this increase in somatic $\Delta F/F$ was lower in magnitude in D2-SPNs than D1-SPNs, it was significant and opposite to amphetamine treatment's effects on somatic D2-SPN Ca^{2+} event rates. Along the same lines, amphetamine treatment decreased both the $\Delta F/F$ and rate of events in bulk D1-SPN Ca^{2+} activity—also opposite to either analysis of somatic D1-SPN Ca^{2+} activity (Figure 4). One caveat is that our experiments did not record the onset of amphetamine's effects, because we did not re-start the recordings until 10 min after amphetamine treatment. Nevertheless, pragmatically, the fact that amphetamine treatment decreased the bulk $\Delta F/F$ of both SPN types could explain why it unilaterally increased their somatic $\Delta F/F$—through an overall reduction in background fluorescence. Still, it is unclear why amphetamine treatment suppressed bulk Ca^{2+} activity in D1-SPNs. Further studies are necessary to determine the precise relationships between neuropil and somatic Ca^{2+} activity, whether this differs between the two SPN types, and how this relationship is altered by drug treatment. Delineating these processes would bolster the utility of bulk and somatic recordings of in vivo Ca^{2+} activity for drug screening by associating the readouts with biological insights.

The current study established that the different scales of analysis yield discrete results, which is a first step toward this process. For example, it would be informative to examine the in vivo relationships between dendritic and somatic SPN Ca^{2+} activity with more spatial resolution. Doing so would require sparse labeling and two-photon or other imaging techniques that avoid the optical aberrations inherent to GRIN lenses (Howe and Dombeck 2016). A key difference between the imaging data in our study and fiber photometry is that we intentionally focus the miniature microscope on cell bodies in the striatum, which may not precisely reflect the bulk signal detected by a fiber optic probe. One potential way to disentangle the differences between the somatic and neuropil components of bulk Ca^{2+} signals would be to compare cytosolic versus soma-targeted variants of GCaMP in response to drug treatment (Grødem et al. 2023).

A key goal of this study was to identify a way to translate between bulk and somatic recordings of Ca^{2+} activity in the context of drug screening. To that end, we normalized and directly compared the effects of amphetamine treatment on D1-SPN and D2-SPN activity as a function of locomotor speed and found that the analysis of bulk Ca^{2+} event rates best recapitulated the data in our previous study (Figures 3–5). Although these data analysis types were not completely congruent, there were some parallels in how they reflected the effect of drug treatment. For instance, except for D1R partial agonist treatment (which, like amphetamine, suppressed D1-SPN bulk Ca^{2+} events), the effects of drugs on D1-SPN activity when administered alone were largely consistent between the two data types (Figure 7). Likewise, except for pretreatment with the non-antipsychotic drug MP-10 (a phosphodiesterase 10a inhibitor), the effects of drug + amphetamine treatment on bulk and somatic D2-SPN Ca^{2+} activity were largely consistent (Figure 6). However, the effects of drug-alone treatment on D2-SPN Ca^{2+} activity and drug + amphetamine treatment on D1-SPN Ca^{2+} activity were highly inconsistent between the analyses of bulk and somatic event rates. Nevertheless, because there were consistent effects between the bulk and somatic data under drug-alone treatment in D1-SPNs and drug + amphetamine treatment in D2-SPNs, the indices of dopamine state-dependent effects were qualitatively similar, though more variable in the bulk Ca^{2+} event data (Figure 8). Notably, both data analysis modalities

underscored the state-dependent modulation of D1-SPN activity as a key indicator of clinical antipsychotic efficacy.

In summary, our comparison of bulk versus somatic Ca^{2+} signaling in the striatum revealed important differences for consideration by groups aiming to deploy this technique to read out the actions of drugs in the brain. On the one hand, these differences likely reflect distinct biological processes that offer new perspectives on how drugs act on the brain. On the other, they underscore the potential pitfalls of equating bulk and cellular-resolution imaging data. Exploring these different data analysis types in our own study allowed us to identify steps to better align the effects of antipsychotic drug treatment on D1-SPN and D2-SPN activity (i.e., event detection and state-dependent analysis). However, more studies are necessary to understand the biological processes underlying the differences between these data analyses to fully leverage the differences for drug screening. Nevertheless, when the differences identified in this study are taken into consideration, these techniques offer a powerful neural phenotypic screening approach with great potential for advancing drug discovery.

Author contributions

S.Y. and J.G.P. designed and performed all experiments, conducted all data analyses, and wrote the manuscript.

Acknowledgments

S.Y. and J.G.P. were funded by NIMH K01MH11313201, NINDS R01NS122840, and the Whitehall Foundation.

Conflicts of Interest

The authors declare no conflicts of interest.

Data Availability Statement

The data that support the findings of this study are available on request from the corresponding author. The data are not publicly available due to privacy or ethical restrictions.

References

Abi-Dargham, A., J. Rodenhiser, D. Printz, et al. 2000. "Increased Baseline Occupancy of D2 Receptors by Dopamine in Schizophrenia." *Proceedings of the National Academy of Sciences of the United States of America* 97, no. 14: 8104–8109. https://doi.org/10.1073/pnas.97.14.8104.

Aharoni, D., B. S. Khakh, A. J. Silva, and P. Golshani. 2019. "All the Light That We Can See: A New Era in Miniaturized Microscopy." *Nature Methods* 16, no. 1: 11–13. https://doi.org/10.1038/s41592-018-0266-x.

Blay, V., B. Tolani, S. P. Ho, and M. R. Arkin. 2020. "High-Throughput Screening: Today's Biochemical and Cell-Based Approaches." *Drug Discovery Today* 25, no. 10: 1807–1821. https://doi.org/10.1016/j.drudis.2020.07.024.

Corder, G., B. Ahanonu, B. F. Grewe, D. Wang, M. J. Schnitzer, and G. Scherrer. 2019. "An Amygdalar Neural Ensemble That Encodes the Unpleasantness of Pain." *Science* 363, no. 6424: 276–281. https://doi.org/10.1126/science.aap8586.

Creese, I., D. R. Burt, and S. H. Snyder. 1996. "Dopamine Receptor Binding Predicts Clinical and Pharmacological Potencies of Antischizophrenic Drugs." *Journal of Neuropsychiatry and Clinical Neurosciences* 8, no. 2: 223–226. https://doi.org/10.1176/jnp.8.2.223.

Cui, G., S. B. Jun, X. Jin, et al. 2013. "Concurrent Activation of Striatal Direct and Indirect Pathways During Action Initiation." *Nature* 494, no. 7436: 238–242. https://doi.org/10.1038/nature11846.

Cui, G., S. B. Jun, X. Jin, et al. 2014. "Deep Brain Optical Measurements of Cell Type-Specific Neural Activity in Behaving Mice." *Nature Protocols* 9, no. 6: 1213–1228. https://doi.org/10.1038/nprot.2014.080.

Dong, C., Y. Zheng, K. Long-Iyer, E. C. Wright, Y. Li, and L. Tian. 2022. "Fluorescence Imaging of Neural Activity, Neurochemical Dynamics, and Drug-Specific Receptor Conformation With Genetically Encoded Sensors." *Annual Review of Neuroscience* 45: 273–294. https://doi.org/10.1146/annurev-neuro-110520-031137.

Ghosh, K. K., L. D. Burns, E. D. Cocker, et al. 2011. "Miniaturized Integration of a Fluorescence Microscope." *Nature Methods* 8, no. 10: 871–878. https://doi.org/10.1038/nmeth.1694.

Grødem, S., I. Nymoen, G. H. Vatne, et al. 2023. "An Updated Suite of Viral Vectors for in Vivo Calcium Imaging Using Intracerebral and Retro-Orbital Injections in Male Mice." *Nature Communications* 14, no. 1: 608. https://doi.org/10.1038/s41467-023-36324-3.

Hirano, K., Y. Morishita, M. Minami, and H. Nomura. 2022. "The Impact of Pitolisant, an H(3) Receptor Antagonist/Inverse Agonist, on Perirhinal Cortex Activity in Individual Neuron and Neuronal Population Levels." *Scientific Reports* 12, no. 1: 7015. https://doi.org/10.1038/s41598-022-11032-y.

Howe, M. W., and D. A. Dombeck. 2016. "Rapid Signalling in Distinct Dopaminergic Axons During Locomotion and Reward." *Nature* 535, no. 7613: 505–510. https://doi.org/10.1038/nature18942.

Huhn, M., A. Nikolakopoulou, J. Schneider-Thoma, et al. 2019. "Comparative Efficacy and Tolerability of 32 Oral Antipsychotics for the Acute Treatment of Adults With Multi-Episode Schizophrenia: A Systematic Review and Network Meta-Analysis." *Lancet* 394, no. 10202: 939–951. https://doi.org/10.1016/s0140-6736(19)31135-3.

Lange, J. H., J. H. Reinders, J. T. Tolboom, J. C. Glennon, H. K. Coolen, and C. G. Kruse. 2007. "Principal Component Analysis Differentiates the Receptor Binding Profiles of Three Antipsychotic Drug Candidates From Current Antipsychotic Drugs." *Journal of Medicinal Chemistry* 50, no. 21: 5103–5108. https://doi.org/10.1021/jm070516u.

Legaria, A. A., B. A. Matikainen-Ankney, B. Yang, et al. 2022. "Fiber Photometry in Striatum Reflects Primarily Nonsomatic Changes in Calcium." *Nature Neuroscience* 25, no. 9: 1124–1128. https://doi.org/10.1038/s41593-022-01152-z.

Manning, E. E., M. A. Geramita, S. C. Piantadosi, J. L. Pierson, and S. E. Ahmari. 2023. "Distinct Patterns of Abnormal Lateral Orbitofrontal Cortex Activity during Compulsive Grooming and Reversal Learning Normalize After Fluoxetine." *Biological Psychiatry* 93, no. 11: 989–999. https://doi.org/10.1016/j.biopsych.2021.11.018.

Marshall, J. J., J. Xu, N.-H. Yeh, et al. 2024. "Synaptic Mechanisms Modulate the Spatiotemporal Dynamics of Striatal Direct Pathway Neurons and Motor Output." *eLife* 13: RP98122.

McCutcheon, R. A., A. Abi-Dargham, and O. D. Howes. 2019. "Schizophrenia, Dopamine and the Striatum: From Biology to Symptoms." *Trends in Neurosciences* 42, no. 3: 205–220. https://doi.org/10.1016/j.tins.2018.12.004.

Moya, N. A., S. Yun, S. W. Fleps, et al. 2023. "The Effect of Selective Nigrostriatal Dopamine Excess on Behaviors Linked to the Cognitive and Negative Symptoms of Schizophrenia." *Neuropsychopharmacology* 48, no. 4: 690–699. https://doi.org/10.1038/s41386-022-01492-1.

Olten, B., and M. H. Bloch. 2018. "Meta Regression: Relationship Between Antipsychotic Receptor Binding Profiles and Side-Effects." *Progress in Neuro-Psychopharmacology and Biological Psychiatry* 84, no. Pt A: 272–281. https://doi.org/10.1016/j.pnpbp.2018.01.023.

Parker, J. G., J. D. Marshall, B. Ahanonu, et al. 2018. "Diametric Neural Ensemble Dynamics in Parkinsonian and Dyskinetic States." *Nature* 557, no. 7704: 177–182. https://doi.org/10.1038/s41586-018-0090-6.

Patriarchi, T., J. R. Cho, K. Merten, et al. 2018. "Ultrafast Neuronal Imaging of Dopamine Dynamics With Designed Genetically Encoded Sensors." *Science* 360, no. 6396: eaat4422. https://doi.org/10.1126/science.aat4422.

Seeman, P., T. Lee, M. Chau-Wong, and K. Wong. 1976. "Antipsychotic Drug Doses and Neuroleptic/Dopamine Receptors." *Nature* 261, no. 5562: 717–719. https://doi.org/10.1038/261717a0.

Spark, D. L., A. Fornito, C. J. Langmead, and G. D. Stewart. 2022. "Beyond Antipsychotics: A Twenty-First Century Update for Preclinical Development of Schizophrenia Therapeutics." *Translational Psychiatry* 12, no. 1: 147. https://doi.org/10.1038/s41398-022-01904-2.

Thevenaz, P., U. E. Ruttimann, and M. Unser. 1998. "A Pyramid Approach to Subpixel Registration Based on Intensity." *IEEE Transactions on Image Processing: A Publication of the IEEE Signal Processing Society* 7, no. 1: 27–41. https://doi.org/10.1109/83.650848.

Yun, S., B. Yang, J. D. Anair, et al. 2023. "Antipsychotic Drug Efficacy Correlates With the Modulation of D1 Rather Than D2 Receptor-Expressing Striatal Projection Neurons." *Nature Neuroscience* 26, no. 8: 1417–1428. https://doi.org/10.1038/s41593-023-01390-9.

Zhang, Y., M. Rózsa, Y. Liang, et al. 2023. "Fast and Sensitive GCaMP Calcium Indicators for Imaging Neural Populations." *Nature* 615, no. 7954: 884–891. https://doi.org/10.1038/s41586-023-05828-9.

Supporting Information

Additional supporting information can be found online in the Supporting Information section.